Generation of non-diffractive Bessel beams by inward cylindrical traveling wave aperture distributions

M. Albani,[1] **S. C. Pavone,**[1] **M. Casaletti,**[2] **and M. Ettorre**[3,*]

[1]*Dipartimento di Ingegneria dell'Informazione e Scienze Matematiche, Università di Siena, via Roma 56, 53100, Siena, Italy*

[2]*Laboratoire d'Electronique et Electromagnétisme, Université Pierre et Marie Curie - Paris 6, 75005 Paris, France*

[3]*Institut d'Electronique et de Télécommunications de Rennes, UMR CNRS 6164, Université de Rennes 1, 35042 Rennes Cedex, France*

[*]*mauro.ettorre@univ-rennes1.fr*

Abstract: The focusing capabilities of an inward cylindrical traveling wave aperture distribution and the non-diffractive behaviour of its radiated field are analyzed. The wave dynamics of the infinite aperture radiated field is clearly unveiled by means of closed form expressions, based on incomplete Hankel functions, and their ray interpretation. The non-diffractive behaviour is also confirmed for finite apertures up to a defined limited range. A radial waveguide made by metallic gratings over a ground plane and fed by a coaxial feed is used to validate numerically the analytical results. The proposed system and accurate analysis of non-diffractive Bessel beams launched by inward waves opens new opportunities for planar, low profile beam generators at microwaves, Terahertz and optics.

OCIS codes: (050.1960) Diffraction theory; (350.5500) Propagation; (050.1220) Apertures.

References and links

1. J. Durnin, "Exact solutions for nondiffracting beams. I. The scalar theory," J. Opt. Soc. Am. A **4**, 651–654 (1987).
2. J. Durnin, J. J. Miceli, Jr., and J. H. Eberly, "Diffraction-free beams," Phys. Rev. Lett. **58**, 1499 (1987).
3. M. Lapointe, "Review of non-diffracting Bessel beam experiments," Opt. Laser Technol. **24**, 315–321 (1992).
4. J. Arlt and K. Dholakia, "Generation of high-order Bessel-beams by use of an axicon," Opt. Commun. **177**, 297–301 (2000).
5. R. M. Herman and T. A. Wiggins, "Production and uses of diffracionless beams," J. Opt. Soc. Am. A **8**, 932–942 (1991).
6. Z. Li, K. B. Alici, H. Caglayan, and E. Ozbay, "Generation of an axially asymmetric Bessel-like beam from a metallic subwavelength aperture," Phys. Rev. Lett. **102**, 143901 (2009).
7. W. B. Williams and J. B. Pendry, "Generating Bessel beams by use of localized modes," J. Opt. Soc. Am. A **22**, 992–997 (2005).
8. A. Mazzinghi, M. Balma, D. Devona, G. Guarnieri, G. Mauriello, M. Albani, and A. Freni, "Large depth of field pseudo-Bessel beam generation with a RLSA antenna," IEEE Trans. Antennas Propag. (to be published).
9. J. C. Gutiérrez-Vega, M. D. Iturbe-Castillo, and S. Chávez-Cerda, "Alternative formulation for invariant optical fields: Mathieu beams," Opt. Lett. **25**, 1493–1495 (2000).
10. J. Salo, J. Fagerholm, A. T. Friberg, and M. M. Salomaa, "Unified description of nondiffracting X and Y waves," Phys. Rev. A **62**, 4261 (2000).
11. M. Anguiano-Morales, M. M. Méndez-Otero, M. D. Iturbe-Castillo, and S. Chávez-Cerda, "Near field diffraction of Hankel beams," in *Frontiers in Optics*, OSA Technical Digest (CD) (Optical Society of America, 2006), paper JSuA36.

#211702 - $15.00 USD Received 14 May 2014; revised 12 Jun 2014; accepted 17 Jun 2014; published 22 Jul 2014

12. M. Ettorre and A. Grbic, "Generation of propagating Bessel beams using leaky-wave modes," IEEE Trans. Antennas Propag. **60**, 3605–3613 (2012).
13. M. Ettorre, S. M. Rudolph, and A. Grbic, "Generation of propagating Bessel beams using leaky-wave modes: experimental validation," IEEE Trans. Antennas Propag. **60**, 2645–2653 (2012).
14. M. F. Inami and A. Grbic, "Generating Bessel beams using an electrically-large annular slot," in *Proceedings of IEEE AP-S/URSI-USNC Symposium* (IEEE 2013).
15. S. Chávez-Cerda, "A new approach to Bessel beams," J. Mod. Opt. **46**, 923–930 (1999).
16. S. Chávez-Cerda and G. H. C. New, "Evaluation of focused Hankel waves and Bessel beams," Opt. Commun. **181**, 369–377 (2000).
17. J. Lin, J. Dellinger, P. Genevet, B. Cluzel, F. de Fornel, and F. Capasso, "Cosine-Gauss plasmon beam: a localized long-range nondiffracting surface wave," Phys. Rev. Lett. **109**, 093904 (2012).
18. L. B. Felsen and N. Marcuvitz, *Radiation and Scattering of Waves*, Series on Electromagnetic Wave Theory (IEEE Press, 1994).
19. R. Cicchetti and A. Faraone, "Incomplete Hankel and modified Bessel functions: a class of special functions for electromagnetics," IEEE Trans. Antennas Propag. **52**, 3373–3389 (2004).
20. M. Albani, A. Mazzinghi, and A. Freni, "Automatic design of CP-RLSA antennas," IEEE Trans. Antennas Propag. **60**, 5538–5547 (2012).
21. M. Ettorre, M. Casaletti, G. Valerio, R. Sauleau, L. Le Coq, S. C. Pavone, and M. Albani, "On the near-field shaping and focusing capability of a radial line slot array," IEEE Trans. Antennas Propag. **62**, 1991–1999 (2014).

1. Introduction

The spreading of the transverse profile of a propagating wave is an all-present phenomenon known as diffraction. The possibility to limit diffraction spreading over a limited region has been an interesting area of research since the introduction of the so-called non-diffractive Bessel beams [1]. Ideal Bessel beams are solutions to the scalar wave equation that remain confined and do not undergo diffractive spreading but carry infinite power, therefore being nonphysical. Several approaches have been proposed to experimentally generate Bessel beams over finite apertures achieving a non-diffractive behaviour in a limited distance known as non-diffractive range [2]-[8]. During the years, other invariant solutions of the Helmholtz equation have been also proposed and generalized to the polychromatic case [9]-[10]. In addition a series of works [9]-[16] have also highlighted the fact that Bessel beams are cylindrical standing waves generated by the interference of two cylindrical traveling waves, or Hankel beams, one traveling outward and the other inward over the radiating aperture. The combination of the two traveling waves is generally obtained on a small frequency band resulting in a resonant aperture field distribution [12]. The properties of ideal Bessel beams are well established in literature. However, few works have been focusing on their composing cylindrical traveling waves [10] and relative non-diffractive behaviour [11].

Here, the field radiated by inward cylindrical waves traveling over a radiating infinite aperture is expressed in terms of incomplete Hankel functions. The radiated field is split into two main contributions: Geometrical Optics (GO) and Space Wave (SW) arising at the aperture center. Closed form expressions clearly show that the GO contribution creates a non-diffractive Bessel beam radiation close to the axis of symmetry of the generating aperture, where the SW is negligible. Therefore, non-diffractive radiation is not only generated by resonant apertures having a Bessel-like distribution given by a combination of inward and outward cylindrical waves, thus simplifying the beam generator synthesis. In contrast, the case of outward cylindrical wave infinite aperture distribution is also treated by showing that it cannot provide a non-diffractive beam generation. The finite aperture case is then considered for an inward aperture illumination, showing that the non-diffractive Bessel beam is still generated within a given a non-diffractive range, as it happens for finite size Bessel distributions. Finally, to implement the proposed concept, a radial waveguide loaded by metallic gratings and fed by a coaxial feed is used as a beam generator device with an inward cylindrical aperture distribution at microwave frequencies. The coaxial feed within the radial waveguide launches an outward cylindrical wave. The

#211702 - $15.00 USD Received 14 May 2014; revised 12 Jun 2014; accepted 17 Jun 2014; published 22 Jul 2014

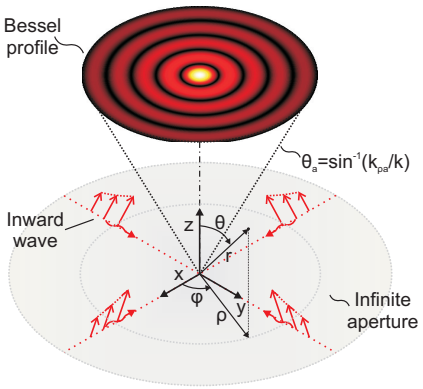

Fig. 1. Schematic view of the considered configuration. The aperture field distribution is a cylindrical inward wave with radial propagation constant $k_{\rho a}$. The non-diffractive zone is limited by the cone with angle $\theta_a = \sin^{-1}(k_{\rho a}/k)$, where k is the free space wavenumber.

position and size of the metallic gratings are properly chosen to sample the outward feeding wave launched by the feed for synthesizing the required inward aperture distribution.

Note that this structure is different from the one proposed in [6], where an incident field generated by an external horn antenna was used to illuminate a subwavelength annular aperture on the back side of a radial waveguide loaded with metallic gratings of same size and periodically placed over the aperture. The presented approach for the analysis and generation of non-diffractive Bessel beams and the proposed simple structure may find several applications in optics and at radio frequencies [5] or for the generation of surface plasmon polaritons [17].

2. Analytical derivation: infinite case

The geometry of the problem is shown in Fig. 1. The origin of the reference system is at the aperture center with the z-axis normal to the aperture. For the sake of convenience, the observation point is expressed either in cylindrical (ρ, ϕ, z) or in spherical (r, θ, ϕ) coordinates; vectors are bold and a hat denotes a unit vector. In the following discussion, Transverse Magnetic (TM) modes with respect to the z-direction will only be considered. However, a similar procedure can be applied to Transverse Electric (TE) modes. An inward cylindrical wave is assumed for the tangential electric field on the radiating aperture: $\mathbf{E_t}(\rho,\phi,z=0) = E_t(\rho,z=0)\hat{\boldsymbol{\rho}} = H_1^{(1)}(k_{\rho a}\rho)\hat{\boldsymbol{\rho}}$. A time dependence $e^{j\omega t}$, $\omega = 2\pi f$ being the angular frequency, is assumed and suppressed. The electric field radiated by the aperture is given by [18]

$$\mathbf{E}(\rho,z) = \frac{1}{4\pi}\int_{\infty e^{-j\pi}}^{+\infty}\left[\frac{k_\rho}{k_z}H_0^{(2)}(k_\rho\rho)\hat{\mathbf{z}} + jH_1^{(2)}(k_\rho\rho)\hat{\boldsymbol{\rho}}\right]\widetilde{E}_t(k_\rho)e^{-jk_z z}k_\rho dk_\rho, \qquad (1)$$

$$\widetilde{E}_t(k_\rho) = -2\pi j\int_0^{+\infty} E_t(\rho,z=0)J_1(k_\rho\rho)\rho d\rho, \qquad (2)$$

where k_ρ, and $k_z = \sqrt{k^2 - k_\rho^2}$ are the transverse and longitudinal spectral variables, k is the wavenumber in free space, whereas $J_n()$ and $H_n^{(i)}()$ are the n-th order Bessel and Hankel functions of the i-th kind, respectively. Equation (2) is the Hankel-transform of the tangential field distribution over the aperture and, for the assumed inward cylindrical wave distribution, it is

#211702 - $15.00 USD Received 14 May 2014; revised 12 Jun 2014; accepted 17 Jun 2014; published 22 Jul 2014

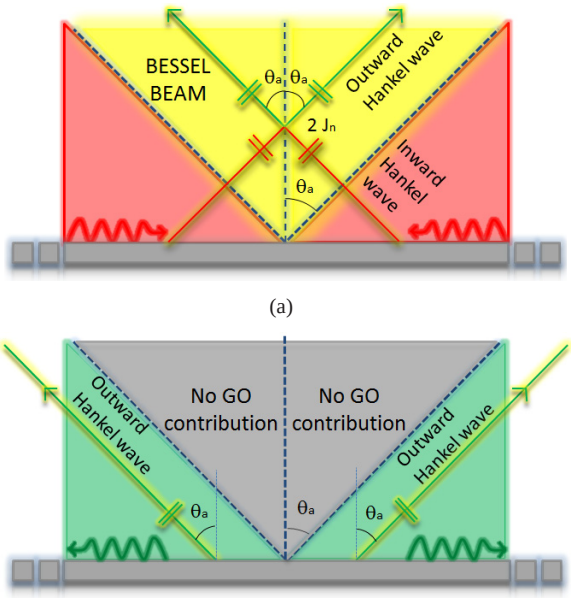

Fig. 2. Ray interpretation of the GO field for an infinite aperture. (a) Inward Hankel aperture distribution: the GO field comprises an inward Hankel beam ray (in red), present throughout the space, and an outward Hankel beam ray (in green) bounded inside the cone $\theta < \theta_a$; the superposition of the two rays inside the cone (yellow area) creates a Bessel beam. (b) Outward Hankel aperture distribution: the GO field comprises only an outward Hankel beam ray (in green) bounded outside the cone $\theta < \theta_a$.

given by

$$\widetilde{E}_t(k_\rho) = \frac{-4k_\rho}{k_{\rho a}(k_\rho^2 - k_{\rho a}^2)}. \tag{3}$$

After some mathematical manipulations (refer to the Appendix for more details), the radiated field is exactly expressed as the superposition of the GO and SW contributions

$$\mathbf{E}(\mathbf{r}) = \mathbf{E}^{GO}(\mathbf{r}) + \mathbf{E}^{SW}(\mathbf{r}), \tag{4}$$

with

$$\begin{aligned}\mathbf{E}^{GO}(\mathbf{r}) &= 2\left[\frac{k_{\rho a}}{jk_{za}}J_0(k_{\rho a}\rho)\hat{\mathbf{z}} + J_1(k_{\rho a}\rho)\hat{\boldsymbol{\rho}}\right]e^{-jk_{za}z}\mathrm{U}(\theta_a - \theta) \\ &\quad + \left[\frac{k_{\rho a}}{jk_{za}}H_0^{(1)}(k_{\rho a}\rho)\hat{\mathbf{z}} + H_1^{(1)}(k_{\rho a}\rho)\hat{\boldsymbol{\rho}}\right]e^{-jk_{za}z}\mathrm{U}(\theta - \theta_a),\end{aligned} \tag{5}$$

$$\begin{aligned}\mathbf{E}^{SW}(\mathbf{r}) &= -\frac{k_{\rho a}}{jk_{za}}\left[\mathrm{sgn}(w_0^-)H_0^{(2)}(k_{\rho a}\rho, |w_0^-|)e^{-jk_{za}z} - H_0^{(2)}(k_{\rho a}\rho, w_0^+)e^{jk_{za}z}\right]\hat{\mathbf{z}} \\ &\quad - \left[\mathrm{sgn}(w_0^-)H_1^{(2)}(k_{\rho a}\rho, |w_0^-|)e^{-jk_{za}z} + H_1^{(2)}(k_{\rho a}\rho, w_0^+)e^{jk_{za}z}\right]\hat{\boldsymbol{\rho}} \\ &\quad - \frac{2}{j\pi k_{\rho a}}(\hat{\mathbf{z}} + \cot\theta\hat{\boldsymbol{\rho}})\frac{e^{-jkr}}{r}\end{aligned}$$

#211702 - $15.00 USD Received 14 May 2014; revised 12 Jun 2014; accepted 17 Jun 2014; published 22 Jul 2014

$$\sim \quad \frac{2\sin\theta}{j\pi k_{\rho a}(\cos^2\theta-\cos^2\theta_a)}\frac{e^{-jkr}}{r}\hat{\boldsymbol{\theta}}, \tag{6}$$

with $k_{za}=\sqrt{k^2-k_{\rho a}^2}$ denoting the Bessel beam normal propagation constant. In Eq. (6), $H_n^{(i)}(\Omega,w_0)$ are the n-th order incomplete Hankel functions of i-th kind with the second argument $w_0^{\pm}=\tanh^{-1}\cos\theta\pm\tanh^{-1}\cos\theta_a$ [19], whereas sgn() and U() are the sign and Heaviside step function, respectively.

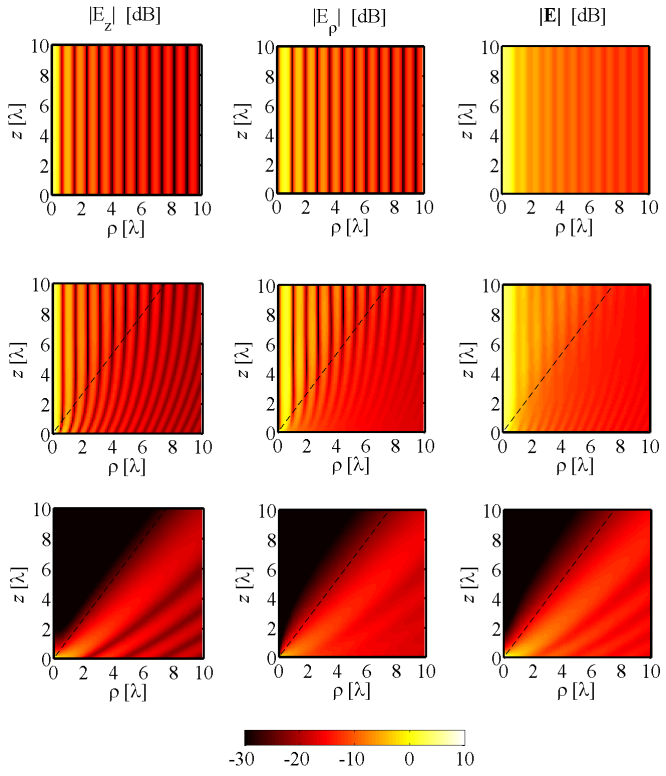

Fig. 3. Electric field radiated by an infinite aperture. $|E_z|$ (1st column), $|E_\rho|$ (2nd column) and total electric field amplitude $|\boldsymbol{E}|$ (3rd column). Standard Bessel beam reference field (1st row), field radiated by an inward Hankel distribution (2nd row), and field radiated by an outward Hankel distribution (3rd row). The axes are normalized with respect to the wavelength (λ) at the operating frequency f. The dashed line marks the GO boundary $\theta=\theta_a$.

The GO contribution exhibits the well-known Bessel beam shape (first term in Eq. (5)) within the cone $\theta<\theta_a$ where $U(\theta_a-\theta)=1$, whereas becomes an inward Hankel beam outside such a cone where $U(\theta_a-\theta)=0$. By considering the Bessel function as the superposition of two Hankel functions $2J_n=H_n^{(1)}+H_n^{(2)}$, GO is interpreted as the superposition of two ray contributions; namely, an inward Hankel beam conical wave is associated to a ray arising from a point on the aperture, and an outward Hankel beam conical wave associated to a ray arising from a point on the aperture which is diametrally opposite with respect to the observation point. Indeed, the launched inward conical wave becomes an outward conical wave beyond the caustic

#211702 - $15.00 USD Received 14 May 2014; revised 12 Jun 2014; accepted 17 Jun 2014; published 22 Jul 2014

at the z-axis. While the former ray reaches the observation point regardless its location, the latter exists only when observing inside the cone $\theta < \theta_a$ (Fig. 2(a)). At the GO discontinuity cone $\theta = \theta_a$, the SW contribution (Eq. (6)) exhibits an opposite abrupt discontinuity which renders the total field smooth and continuous. Such a transitional behaviour is described by the sign and incomplete Hankel functions when $w_0^- \to 0$. Outside the transition region near the discontinuity cone, the SW contribution exhibits a ray-optical behaviour which is derived from the asymptotic expression of incomplete Hankel functions for large arguments [19], and reported in the last line of Eq. (6). Indeed, the SW is a transverse (i.e., $\hat{\boldsymbol{\theta}}$ polarized) spherical wave associated to a ray launched at the aperture center (origin of the reference system in Fig. 1), with a radiation null on the aperture symmetry axis $\theta = 0$.

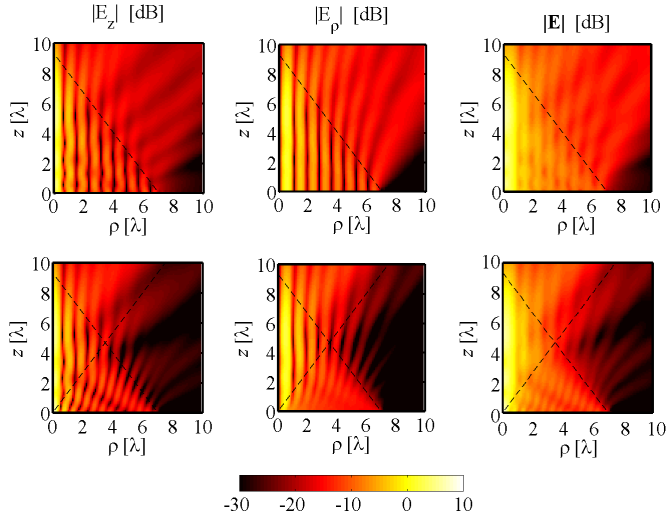

Fig. 4. Electric field radiated by an finite aperture with radius of $a = 7\lambda$. $|E_z|$ (1st column), $|E_\rho|$ (2nd column) and total electric field amplitude $|\boldsymbol{E}|$ (3rd column). Standard Bessel beam reference field (1st row), and field radiated by an inward Hankel distribution (2nd row). The axes are normalized with respect to the wavelength (λ) at the operating frequency f. The dashed line marks the GO boundaries.

As an example, Fig. 3 shows the amplitude of the z (1st column) and ρ (2nd column) components and the total electric field (3rd column) radiated by an inward cylindrical wave (2nd row) with $k_{\rho a} = 0.6k$ in the vertical $z-\rho$ plane. As clear from the previous results, the non diffractive behaviour of the radiated field can be appreciated within the cone with angle $\theta_a \approx 37^\circ$ (dotted line) where the various components of the electric field recover the respective components of a standard Bessel beam (1st row).

On the other hand, by repeating the same formulation for the case of an outward traveling wave over the radiating aperture $\mathbf{E_t}(\rho,\phi,z=0) = H_1^{(2)}(k_{\rho a}\rho)\hat{\boldsymbol{\rho}}$, the radiated field is found again as in Eq. (4) with the following expression for the GO contribution

$$\mathbf{E}^{GO}(\mathbf{r}) \quad = \quad \left[\frac{k_{\rho a}}{jk_{za}} H_0^{(2)}(k_{\rho a}\rho)\hat{\boldsymbol{z}} + H_1^{(2)}(k_{\rho a}\rho)\hat{\boldsymbol{\rho}}\right] e^{-jk_{za}z}\mathrm{U}(\theta-\theta_a), \tag{7}$$

and a SW contribution which is the negative of that in Eq. (6). In Eq. (7), differently from Eq. (5), the GO field contribution is constituted by only a single outward Hankel beam conical

#211702 - $15.00 USD Received 14 May 2014; revised 12 Jun 2014; accepted 17 Jun 2014; published 22 Jul 2014

wave, which however vanishes within the cone delimited by $\theta < \theta_a$. Its ray interpretation is shown in Fig. 2(b). Again, the SW contribution discontinuity perfectly matches the GO jump at the shadow boundary cone, thus providing a smooth continuous total field. Therefore, it is apparent that an outward Hankel distribution cannot produce a Bessel beam, as also clear from Fig. 3(c).

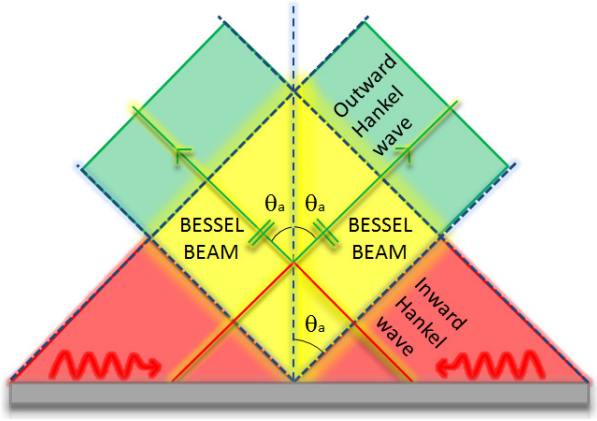

Fig. 5. Ray interpretation of the GO field for an finite aperture. The dashed lines indicated the GO boundaries. The GO contribution is limited in a triangular region with a side corresponding to the finite aperture. The GO field comprises an inward Hankel beam ray (in red), present throughout this triangular region, and an outward Hankel beam ray (in green) bounded inside the cone $\theta < \theta_a$; the superposition of the two rays creates a Bessel beam inside a zone with rhomboidal cross section (yellow area).

3. Finite case

Once established the capabilities of generating a non-diffractive wave for theoretical infinite apertures, the field radiated by a finite aperture with an inward cylindrical traveling wave distribution has been then considered for assessing the practical finite case. Equation (1) is still valid once the Hankel-transform of the tangential field distribution over the finite aperture is considered:

$$\widetilde{E}_t(k_\rho) = \frac{-4}{k_\rho^2 - k_{\rho a}^2}\left[\frac{k_\rho}{k_{\rho a}} + \frac{\pi a}{2j}\left(k_\rho H_1^{(1)}(k_{\rho a}a)J_0(k_\rho a) - k_{\rho a}H_0^{(1)}(k_{\rho a}a)J_1(k_\rho a)\right)\right]. \quad (8)$$

Since for the finite aperture case a closed form field expression is not available, the electric field is then evaluated numerically through Eq. (1). As an example, the field map for an aperture of radius $a = 7\lambda$ (refer to Fig. 1) is shown in Fig. 4. Analogously to Fig. 3, z, ρ components and total electric field are arranged in the 1st, 2nd, and 3rd column, respectively; while the results for a Bessel, and inward Hankel aperture distributions are arranged in the 1st, 2nd row, respectively. In both cases k_a is equal to $0.6k$. In the present finite case additional GO shadow boundaries (dotted lines) arise from the aperture rim and limit the GO contribution in a conical region above the aperture with vertex on the z-axis at a distance $z = a\cot\theta_a \simeq 9.33\lambda$, as shown in Fig. 5; hence the non-diffractive behaviour is limited up to this distance for both the reference Bessel [1] and the inward Hankel distributions. In the latter case the Bessel beam is generated in the region between the two conical boundaries which exhibits a rhomboidal cross section, in contrast to the well known triangular cross section of the reference case.

#211702 - $15.00 USD Received 14 May 2014; revised 12 Jun 2014; accepted 17 Jun 2014; published 22 Jul 2014

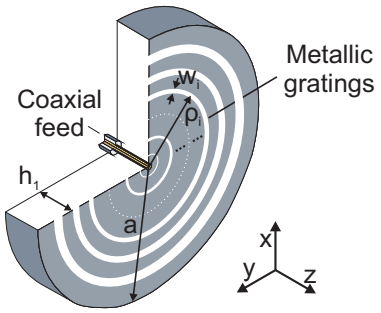

Fig. 6. Radial waveguide loaded with metallic gratings and fed by a coaxial fed.

Table 1. Geometrical sizes of the Bessel beam launcher: radial positions (ρ_i) and widths (w_i) of the annular slots. The PPW is filled with a dielectric with permittivity 2.2 and thickness $h_1 = 3.175$ mm.

Slot	ρ_i [mm]	w_i [mm]	Slot	ρ_i [mm]	w_i [mm]
1	1.5	0.55	7	110	2.3
2	29.8	0.94	8	126.5	2.6
3	45.7	1.1	9	143	3
4	61.5	1.5	10	159.5	3.5
5	76.4	1.2	11	175.4	3.8
6	94.1	3	12	192.4	4

However the depth of focus of the two distributions, i.e the non-diffractive range, is the same, and the shape of the realized beam close to the z-axis is very similar. This demonstrates that the capability of an inward Hankel aperture distribution of launching a Bessel beam is practically equivalent to that of the standard Bessel distribution.

4. Proposed structure: radial waveguide loaded with metallic gratings

The practical implementation of a Bessel beam launcher exploiting an inward traveling wave aperture distribution, is shown in Fig. 6. The structure is made by a parallel-plate waveguide (PPW) with annular slots etched on the top plate (Fig. 6). A coaxial feed at the center excites an outward cylindrical radial wave inside the PPW. An in-house Method of Moments (MoM) and the design procedure proposed in [8], [20], [21] was used to tailor the tangential field distribution over the top plate in the shape of an inward cylindrical wave. This is accomplished by controlling the positions along the radial direction ρ_i and sizes w_i of the circular slots (refer to Fig. 6). Indeed, slots are positioned at those points where the phase of the outward cylindrical feeding wave inside the PPW matches that of the target inward cylindrical aperture distribution, according to an holographic criterion. The slot width is used to modulate the amplitude of the aperture distribution. In addition the design procedure assures that the total energy launched by the coaxial feed in the PPW is radiated, thus avoiding any spurious radiation by the edges of the structure. The geometrical details of the structure are provided in Table 1.

COMSOL Multiphysics has been used to analyze the structure. Field maps of the electric field above the launcher are shown in Fig. 7, which are found very similar to their theoretical counterparts in Fig. 4. To allow a clearer quantitative comparison, we also show in Fig. 8 the

#211702 - $15.00 USD Received 14 May 2014; revised 12 Jun 2014; accepted 17 Jun 2014; published 22 Jul 2014

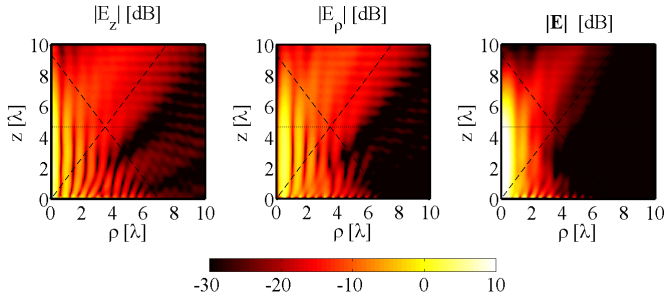

Fig. 7. Electric field radiated by the launcher prototype in Fig. 6, calculated using COMSOL Multiphysics. From left to right, $|E_z|$, $|E_\rho|$ and $|\boldsymbol{E}|$. The axes are normalized with respect to the wavelength (λ) at the operating frequency $f = 10$ GHz. The dashed line marks the GO boundaries and the dotted line refers to the field scan shown in Fig. 8.

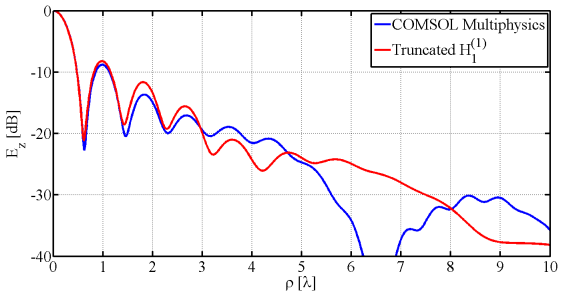

Fig. 8. Normalized $|E_z|$ component of the electric field at $z = 4.667\lambda$ for the structure in Fig. 6 simulated with COMSOL Multiphysics. The field radiated by a truncated inward Hankel distribution is shown for comparison.

E_z component of the electric field at the distance $z = 4.667\lambda$ from the aperture, corresponding to the maximum transverse extension of the rhomboidal region where the Bessel beam is created (dashed line in Fig. 7), compared to the ideal truncated ($a = 7\lambda$) inward Hankel aperture distribution. The good agreement reveals the accuracy of the launcher design. It is worth noting that the traveling nature of the synthesized aperture distribution guarantees a wide-band operation as a difference with resonant Bessel designs [2], [13], [15].

5. Conclusion

In this letter, we have shown that Bessel beams can be created by radiating apertures taking on tangential inward Hankel distributions. The non-diffractive behaviour of such Hankel beams have been investigated theoretically by evaluating the GO and SW field contributions to the total radiated field. In particular, incomplete Hankel functions have been adopted to represent in closed form the SW term. Finally, a Bessel beam launcher based on an inward Hankel distribution was designed to further validate the proposed solution. Future work will consider an experimental validation of the proposed structure in the millimeter wave range. The proposed solution for generating non-diffractive Bessel beams may find application in areas such as near-field communication, radiometry, and non-destructive evaluation.

#211702 - $15.00 USD Received 14 May 2014; revised 12 Jun 2014; accepted 17 Jun 2014; published 22 Jul 2014

Appendix

As first step we consider an outward aperture cylindrical wave distribution $E_t(\rho, z=0) = H_1^{(2)}(k_{\rho a}\rho)$. Equation (1) is recast in the following form

$$\mathbf{E}(\mathbf{r}) = \left[\left(k^2 + \frac{\partial^2}{\partial z^2}\right)\hat{\mathbf{z}} + \frac{\partial^2}{\partial\rho\partial z}\hat{\boldsymbol{\rho}}\right] S(\mathbf{r}) \tag{9}$$

in which the electric field is obtained in terms of a Transverse Magnetic (TM) scalar potential

$$S(\mathbf{r}) = \frac{1}{4\pi}\int_{\infty e^{-j\pi}}^{+\infty} \tilde{E}_t(k_\rho) H_0^{(2)}(k_\rho\rho)\frac{e^{-jk_z z}}{k_z} dk_\rho. \tag{10}$$

The Hankel-transform of the tangential field distribution over the aperture for the assumed outward cylindrical wave is the negative of the one in Eq. (3). By expressing the poles of $\tilde{E}_t(k_\rho)$ in an integral form

$$\frac{1}{k_\rho^2 - k_{\rho a}^2} = \frac{1}{2jk_{za}}\left(\int_{-\infty}^{0} e^{j(k_z - k_{za})\zeta} d\zeta - \int_{-\infty}^{0} e^{j(k_z + k_{za})\zeta} d\zeta\right), \tag{11}$$

after interchanging the order of the integrals, the spectral k_ρ-integral is closed analytically by means of

$$\frac{1}{2\pi}\int_{-\infty}^{\infty}\frac{1}{4j}\frac{k_\rho}{k_z} H_0^{(2)}(k_\rho\rho) e^{-jk_z z} dk_\rho = \frac{e^{-jk\sqrt{\rho^2+z^2}}}{4\pi\sqrt{\rho^2+z^2}}, \tag{12}$$

resulting in the spatial representation

$$S(\mathbf{r}) = \frac{4}{k_{\rho a}k_{za}}\left(\int_{-\infty}^{0} e^{-jk_{za}\zeta}\frac{e^{-jk\sqrt{\rho^2+(z-\zeta)^2}}}{4\pi\sqrt{\rho^2+(z-\zeta)^2}} d\zeta - \int_{-\infty}^{0} e^{jk_{za}\zeta}\frac{e^{-jk\sqrt{\rho^2+(z-\zeta)^2}}}{4\pi\sqrt{\rho^2+(z-\zeta)^2}} d\zeta\right). \tag{13}$$

Finally, the change of integration variable

$$w = \sinh^{-1}\left(\frac{z-\zeta}{\rho}\right) \mp \tanh^{-1}\left(\frac{k_{za}}{k}\right) \tag{14}$$

is used with the upper/lower sign in the first/second integral of Eq. (13), so that the TM scalar potential reduces to

$$S(\mathbf{r}) = \frac{1}{j\pi k_{\rho a}k_{za}}\left[H_0^{(2)}(k_{\rho a}\rho, w_0^-)e^{-jk_{za}z} - H_0^{(2)}(k_{\rho a}\rho, w_0^+)e^{jk_{za}z}\right], \tag{15}$$

namely the sum of two zero order, second kind incomplete Hankel functions [19]

$$H_0^{(2)}(\Omega, w_0) = \frac{j}{\pi}\int_{w_0}^{+\infty} e^{-j\Omega\cosh w} dw, \tag{16}$$

whose second arguments are

$$w_0^{\pm} = \tanh^{-1}\cos\theta \pm \tanh^{-1}\cos\theta_a, \tag{17}$$

with $\sin\theta_a = k_{\rho a}/k$ and $\cos\theta_a = k_{za}/k$. In the case of an inward cylindrical wave distribution the tangential aperture field can be represented as $E_t(\rho, z=0) = H_1^{(1)}(k_{\rho a}\rho) = 2J_1(k_{\rho a}\rho) -$

#211702 - $15.00 USD Received 14 May 2014; revised 12 Jun 2014; accepted 17 Jun 2014; published 22 Jul 2014

$H_1^{(2)}(k_{\rho a}\rho)$. By noting that the Bessel aperture distribution simply radiates a Bessel beam and by using Eq. (15), it is straightforward to derive the scalar potential as

$$S(\mathbf{r}) = \frac{1}{j\pi k_{\rho a} k_{za}} \left[2J_0(k_{\rho a}\rho, w_0^-) e^{-jk_{za}z} - H_0^{(2)}(k_{\rho a}\rho, w_0^-) e^{-jk_{za}z} + H_0^{(2)}(k_{\rho a}\rho, w_0^+) e^{jk_{za}z} \right]. \tag{18}$$

Now, since $\theta, \theta_a \in [0, \pi/2]$, then $w_0^+ \geq 0$ and the second incomplete Hankel function is asymptotically dominated only by its end-point contribution for any observation point. The same holds for the first incomplete Hankel function only when observing for $\theta \leq \theta_a$ and $w_0^- \geq 0$. Conversely, when $\theta > \theta_a$, then $w_0^- < 0$ and the first incomplete Hankel function asymptotically comprises also a saddle point contribution. To isolate such a contribution one can exploit [19]

$$H_0^{(2)}(\Omega, w_0) = H_0^{(2)}(\Omega) U(w_0) + \mathrm{sgn}(w_0) H_0^{(2)}(\Omega, |w_0|), w_0 \in R \tag{19}$$

and rearrange the expression for the scalar potential S as the sum of a GO and a SW contributions

$$S(\mathbf{r}) = S^{GO}(\mathbf{r}) + S^{SW}(\mathbf{r}), \tag{20}$$

with

$$S^{GO}(\mathbf{r}) = \frac{1}{jk_{\rho a} k_{za}} \left[2J_0(k_{\rho a}\rho) U(\theta_a - \theta) + H_0^{(1)}(k_{\rho a}\rho) U(\theta - \theta_a) \right] e^{-jk_{za}z}, \tag{21}$$

$$S^{SW}(\mathbf{r}) = -\frac{1}{jk_{\rho a} k_{za}} \left[\mathrm{sgn}(w_0^-) H_0^{(2)}(k_{\rho a}\rho, |w_0^-|) e^{-jk_{za}z} - H_0^{(2)}(k_{\rho a}\rho, w_0^+) e^{jk_{za}z} \right]. \tag{22}$$

It is worth noting that although Eq. (18) is already an exact compact closed form for the potential, its exact rearrangement in Eq. (20) better highlights the wave constituents of the total field. Indeed the GO contribution is asymptotically dominated only by the saddle point, whereas the SW is asymptotically dominated only by the end point at any observation aspect. As a matter of fact, the non-uniform asymptotic expression [19]

$$H_0^{(2)}(\Omega, w_0) \sim \frac{e^{-j\Omega \cosh w_0}}{\pi \Omega \sinh w_0}, (\Omega \to \infty, w_0 > 0) \tag{23}$$

reveals the spherical wave nature of the SW arising from the aperture center (spatial end point)

$$S^{SW}(\mathbf{r}) \sim \frac{2}{j\pi k^3 \sin\theta_a (\cos^2\theta - \cos^2\theta_a)} \frac{e^{-jkr}}{r}, (k_{\rho a}\rho \to \infty, \theta \neq \theta_a). \tag{24}$$

A transition region around the shadow boundary at $\theta = \theta_a$ is present, where the non-uniform asymptotic expression (24) fails. By differentiating the TM potential according to Eq. (9), the electric field expressions Eqs. (4)–(6) are finally obtained. The same calculations can be repeated for the field radiated by an infinite aperture distribution taking on an outward Hankel function using the scalar potential in Eq. (15), obtaining the result in Eq. (7).

Acknowledgments

The authors would like to thank the European Science Foundation (NEWFOCUS project), Rennes Métropole (AIS project), and the Ministère des Affaires Etrangéres et Européennes and Campus France (Galileo Projet) for their support and financial contribution.

#211702 - $15.00 USD Received 14 May 2014; revised 12 Jun 2014; accepted 17 Jun 2014; published 22 Jul 2014